Validity of the Rapid Buffering Approximation Near a Point Source of Calcium Ions

Gregory D. Smith,*§ John Wagner,*¶ and Joel Keizer*‡§¶

*Institute of Theoretical Dynamics; ‡Section of Neurobiology, Physiology, and Behavior; §Biophysics Graduate Group; and ¶Graduate Group in Applied Mathematics, University of California, Davis, California 95616 USA

ABSTRACT   In the presence of rapid buffers the full reaction-diffusion equations describing Ca^{2+} transport can be reduced using the rapid buffering approximation to a single transport equation for $[Ca^{2+}]$. Here we simulate the full and reduced equations, exploring the conditions necessary for the validity of the rapid buffering approximation for an isolated Ca^{2+} channel or a cluster of channels. Using a point source and performing numerical simulations of different durations, we quantify the error of the rapid buffering approximation as a function of buffer and source parameters as well as the time and spatial scale set by the resolution of confocal microscopic measurements. We carry out simulations of Ca^{2+} "sparks" and "puffs," both with and without the indicator dye Ca^{2+} Green-1, and find that the rapid buffering approximation is excellent. These calculations also show that the traditional calculation of $[Ca^{2+}]$ from a fluorescence signal may grossly underestimate the true value of $[Ca^{2+}]$ near a source. Finally, we use the full model to simulate the transient Ca^{2+} domain near the pore of an open Ca^{2+} channel in a cell dialyzed with millimolar concentrations of 1,2-bis(2-aminophenoxy)ethane-N, N, N, N-tetraacetic acid or EGTA. In this regime, where the rapid buffering approximation is poor, Neher's equation for the steady-state Ca^{2+} profile is shown to be a reliable approximation adjacent to the pore.

INTRODUCTION

Cytosolic calcium concentrations, $[Ca^{2+}]$, are buffered to low levels in cells by endogenous Ca^{2+}-binding proteins. Indeed, recent experiments in a variety of cell types (Allbritton et al., 1992; Neher and Augustine, 1992; Zhou and Neher, 1993; Tse et al., 1994) suggest that only 1–5% of Ca^{2+} ions in the cytoplasm are free, i.e., not bound to buffers. Whereas the identity and roles of cytosolic buffers are not yet fully understood, the existence of high-affinity buffers has important implications for Ca^{2+} signaling mechanisms (Falke et al., 1994), granule exocytosis (Heinemann et al., 1994), excitation-contraction coupling (Berlin et al., 1994; Cannell et al., 1994, 1995), and a variety of other mechanisms in which changes in $[Ca^{2+}]$ are important. The buffered diffusion of Ca^{2+} is also relevant in a number of experimental protocols, including fluorescence techniques for measuring Ca^{2+} concentrations in situ (Tsien, 1980; Grynkiewicz et al., 1985) and for the examination and manipulation of Ca^{2+} concentrations near open Ca^{2+} channels (Neher, 1986). In these protocols exogenous buffers that possess a wide range of affinities for Ca^{2+} are introduced into cells or organelles, either via membrane soluble modifications of the buffer or via pipette. The affinity of the exogenous buffer for Ca^{2+}, its rate of equilibration, and its diffusion constant can be relevant in these experiments, especially when spatial gradients of Ca^{2+} are significant. Table 1 lists a number of representative endogenous and exogenous cytosolic buffers with approximate values of their physical properties.

We have recently developed a simplified mathematical description of Ca^{2+} diffusion that is valid in the presence of buffers that bind Ca^{2+} rapidly (Wagner and Keizer, 1994), the so-called rapid buffering approximation. Experimental estimates of binding rate constants for endogenous Ca^{2+} buffers in the cytoplasm give equilibration times on the order of a few milliseconds (Neher and Augustine, 1992; Zhou and Neher, 1993). For relatively small gradients, like those seen in Ca^{2+} waves, we have estimated that the rapid buffering approximation should be valid for equilibration times less than about 10 ms (Wagner and Keizer, 1994). Generally speaking, the validity of the rapid buffering approximation requires that the equilibration time of the buffers be much smaller than the time required for Ca^{2+} to diffuse across a region of the size of a typical gradient.

Recently it has been possible to resolve very small domains of Ca^{2+} associated with the opening of one or, perhaps, small clusters of Ca^{2+} channels. Because fluorescence imaging of these Ca^{2+} "domains" (Sherman et al., 1990; Llinás et al., 1992), "puffs" (Parker and Yao, 1991; Yao et al., 1995), or "sparks" (Cheng et al., 1993; Tsugorka et al., 1995), as they have been variously called, has limited spatial resolution, one cannot measure the true Ca^{2+} gradients in these regions. Thus it has been of interest to estimate the spatial Ca^{2+} profile near open Ca^{2+} channels using calculations. This is of particular significance when Ca^{2+} channels are themselves Ca^{2+} sensitive (Fogelson and Zucker, 1985; Simon and Llinás, 1985; Blumenfeld et al., 1992; Stern, 1992; Nowycky and Pinter, 1993), for example, in the case of voltage-gated L-type Ca^{2+} channels (Eckert and Chad, 1984; de Leon et al., 1995), the inositol-1,4,5-trisphosphate (IP_3) receptor (Bezprozvanny and Ehrlich, 1994), and depletion-activated Ca^{2+} currents (Zwei-

TABLE 1 Representative cytosolic Ca^{2+} buffers

Name	k^+ $(\mu M^{-1} s^{-1})$	k^- (s^{-1})	K_d (μM)[‡]	Mol. wt. (kD)	D $(\mu m^2 s^{-1})$[§]	References[*]
Endogenous						
Stationary						
Troponin-C	90, 100	300, 7	3, 0.05–0.07	—	—[¶]	Falke et al., 1994
Sarcolemmal phospholipids	—	—	1100, 13	—	—	Post and Langer, 1992
Mobile						
Calmodulin	500, 100	470, 37	0.9–2.0, 0.2–0.4	17	32	Falke et al., 1994
Calbindin-D_{28K}	20	8.6	0.4–1.0	28	27	Koster et al., 1995
Parvalbumin	6[‖]	1	0.00037	12	36	Falke et al., 1994
Exogenous						
EGTA	1.5	0.3	~0.2[**]	0.38	113	Tsien, 1980
BAPTA	600	100	0.1–0.7	0.63	95	Pethig et al., 1989
Fura-2	600	80–100	0.13–0.60	0.64	95[‡‡]	Pethig et al., 1989
Ca^{2+} Green-1	700	170	0.19–0.25	0.91	84	Eberhard and Erne, 1991
Ca^{2+} Green-1 dextran	~700	~170	0.24–0.35	~70	20	Kao, 1994

[*] For review see Baimbridge et al. (1992), Heizmann and Hunziker (1991), and Kao (1994).

[‡] A range indicates that measurements were made under different experimental conditions; values for distinct binding sites are separated by a comma.

[§] Estimated using $D = k_B T/6\pi\eta R_m$ and $R_m = (3M/4\pi dL)^{1/3}$, i.e., the Stokes-Einstein relation assuming a spherical molecule of density, $d = 1.33$ g/cm^3, and molecular weight, M. The viscosity (η) used is four times that of water at room temperature.

[¶] The troponin complex is immobile because of the its association with actin.

[‖] Even slower physiologically because Mg^{2+} must dissociate (with a time constant of approximately 1 s) before Ca^{2+} can bind (Falke et al., 1994).

[**] EGTA is strongly dependent on pH variation near 7.0 (Kao, 1994).

[‡‡] Blatter and Wier (1990) report 31 μm^2 s^{-1} and suggest that 65–70% of fura-2 is immobilized.

fach and Lewis, 1995), or when voltage-gated Ca^{2+} channels are associated with other Ca^{2+}-sensitive ion channels, as they are in smooth muscle cells (ryanodine receptors; Cannell et al., 1994, 1995) and in hair cells (Ca^{2+}-activated potassium channels; Roberts et al., 1990; Roberts 1993, 1994).

Here we explore the range of validity of the rapid buffering approximation for the calculation of Ca^{2+} domains. This is of interest not only because this approximation speeds up calculations significantly, but because it simplifies the interpretation of calculations. A simplified interpretation is especially important in the presence of mobile buffers, which not only buffer Ca^{2+} but assist in Ca^{2+} transport (Roberts, 1993, 1994; Wagner and Keizer, 1994). These advantages become particularly important when complex phenomena such as calcium waves (Jafri and Keizer, 1995) or multiple release sites are considered. Here we address the time and distance scales on which the rapid buffering approximation is valid for a single source and show when it can be used to estimate Ca^{2+} gradients and the dynamics of Ca^{2+} domains.

EQUATIONS AND NUMERICAL METHODS

Following our previous work (Wagner and Keizer, 1994), we assume buffering reactions

$$B_i + Ca^{2+} \underset{k_i^-}{\overset{k_i^+}{\rightleftharpoons}} CaB_i, \tag{1}$$
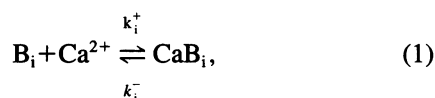
where i = s, m, or e; B_s, B_m, and B_e represent endogenous stationary, endogenous mobile, and exogenous mobile

buffer binding sites, respectively; and CaB_s, CaB_m, and CaB_e represent Ca^{2+} bound to these buffer sites. Assuming mass action kinetics, Fickian diffusion, and a single point source for free Ca^{2+} at the origin ($r = 0$) of a spherical coordinate system, we can write

$$\frac{\partial[Ca^{2+}]}{\partial t} = D_c \nabla^2[Ca^{2+}] - k_s^+[Ca^{2+}][B_s] + k_s^-[CaB_s]$$

$$- \sum_j k_j^+[Ca^{2+}][B_j] + \sum_j k_j^-[CaB_j] + \sigma_0\delta(r), \tag{2}$$

$$\frac{\partial[CaB_s]}{\partial t} = k_s^+[Ca^{2+}][B_s] - k_s^-[CaB_s], \tag{3}$$

$$\frac{\partial[CaB_j]}{\partial t} = D_j\nabla^2[CaB_j] + k_j^+[Ca^{2+}][B_j] - k_j^-[CaB_j], \tag{4}$$

$$\frac{\partial[B_j]}{\partial t} = D_j\nabla^2[B_j] - k_j^+[Ca^{2+}][B_j] + k_j^-[CaB_j]. \tag{5}$$

where j = m or e; D_c is the diffusion constant of Ca^{2+}; D_j is the diffusion constant of B_j and CaB_j (assumed equal); σ_0 is the current amplitude of the source (in units of $\mu mol\ s^{-1}$); the Dirac delta function, $\delta(r)$, is a sharply peaked function at the origin; and B_s is everywhere given by the conservation condition

$$[B_s] = [B_s]_T - [CaB_s], \tag{6}$$

where $[B_s]_T$ is the total concentration of endogenous stationary buffer binding sites. We call this the full model.

If the buffer reactions are fast with respect to the diffusion, and initially the mobile buffers are distributed uniformly, the full model can be reduced to a single transport equation for Ca^{2+} (Wagner and Keizer, 1994),

$$\frac{\partial[Ca^{2+}]}{\partial t} = \beta \left[\nabla^2 \left(D_c[Ca^{2+}] + \sum_j D_j[CaB_j] \right) + \sigma_0 \delta(r) \right], \quad (7)$$

where

$$\beta = \left(1 + \frac{K_s[B_s]_T}{(K_s + [Ca^{2+}])^2} + \sum_j \frac{K_j[B_j]_T}{(K_j + [Ca^{2+}])^2} \right)^{-1} \quad (8)$$

and

$$[CaB_j] = \frac{[B_j]_T[Ca^{2+}]}{K_j + [Ca^{2+}]}. \quad (9)$$

In these equations, which we call the reduced model, $K_i = k_i^-/k_i^+$ are the dissociation constants of the buffer reactions and $[B_s]_T$, $[B_m]_T$, and $[B_e]_T$ are the total concentrations of the buffer binding sites. Although Eqs. 7–9 are most useful for numerical calculations, Eqs. 7 and 9 can be combined to yield an even simpler equation (Wagner and Keizer, 1994),

$$\frac{\partial[Ca^{2+}]}{\partial t} = \beta \left[\left(D_c + \sum_j \gamma_j D_j \right) \nabla^2[Ca^{2+}] \right.$$

$$\left. - 2 \left(\sum_j \frac{\gamma_j D_j}{K_j + [Ca^{2+}]} \right) \nabla[Ca^{2+}] \cdot \nabla[Ca^{2+}] + \sigma_0 \delta(r) \right], \quad (10)$$

where

$$\gamma_j = \frac{K_j[B_j]_T}{(K_j + [Ca^{2+}])^2}. \quad (11)$$

The assumption of rapid equilibrium used in deriving these equations requires that the equilibration time scales for the buffers (τ_i) be rapid with respect to the diffusive time scale. This requirement can be written as (Wagner and Keizer, 1994).

$$\tau_i = \frac{1}{k_i^- + k_i^+([Ca^{2+}] + [B_i])} \ll \frac{L^2}{D_c}, \quad (12)$$

where L is a length characteristic of the spatial profile of Ca^{2+}.

In this paper we investigate buffered Ca^{2+} diffusion near a point source releasing free Ca^{2+} into a three-dimensional hemispherical space using standard spherical coordinates ($0 < r < R_{max}$, $0 < \phi < 2\pi$, and $0 < \theta < \pi/2$) with a no-flux boundary condition at $\theta = \pi/2$. This boundary represents the biological membrane in which the source or channel resides and is assumed to have no curvature and to be impermeable to Ca^{2+} everywhere, except at the location of the channel ($r = 0$). Because we consider only one source for free Ca^{2+}, solutions to both the full and the reduced

models have hemispherical symmetry and the flux of each mobile species lacks a θ or a ϕ component. This implies that solutions to Eqs. 2–5 and Eq. 7 in a sphere of radius R_{max}, but with no boundary at $\theta = \pi/2$ and twice the source strength, are also solutions to these equations in the hemisphere in the presence of the boundary (Carslaw and Jaeger, 1959; Crank, 1975; Stern, 1992). Our calculations utilize this fact. The initial condition for Ca^{2+} in both the full and reduced calculations is $[Ca^{2+}] = c_0$, a uniform background concentration. In the full model calculations, all buffers are assumed initially to be in equilibrium with Ca^{2+}, and these concentrations are also used in a Dirichlet (absorbing) boundary condition for each variable at $r = R_{max}$. In all calculations, R_{max} was chosen large enough that it did not influence the numerical results. The methods used in solving these equations are described in the Appendix.

CONVERGENCE OF THE REDUCED MODEL TO THE FULL MODEL

Fig. 1 shows calculated concentration profiles of free Ca^{2+} and buffer species 1 ms after turning on a 5-pA source. Simulations with the full model (Fig. 1 A) are based on Eqs. 2–5. Physiologically realistic parameters (see legend to Fig.
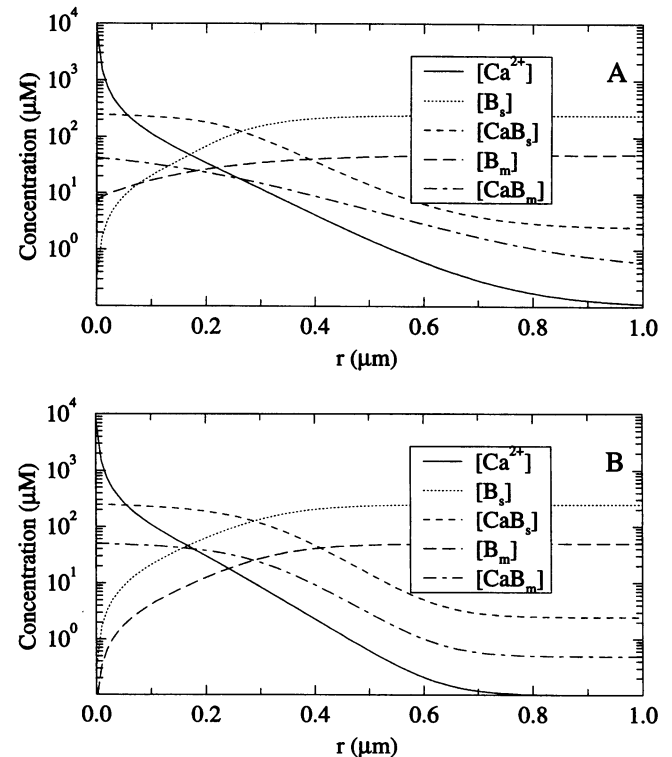

FIGURE 1   (A) Representative full model calculation of $[Ca^{2+}]$ profile near a point source for free Ca^{2+}. Source amplitude (σ_0) and elapsed time (t_0) are 5 pA and 1 ms, respectively. Other parameters: $[B_s]_T = 250 \mu M$; $[B_m]_T = 50 \mu M$; $k_s^- = k_m^- = 10^3 s^{-1}$; $k_s^+ = k_m^+ = 10^2 \mu M^{-1} s^{-1}$; $D_c = 250 \mu m^2 s^{-1}$; $D_m = 75 \mu m^2 s^{-1}$; $\Delta t = 0.1 \mu s$; $\Delta r = 0.01 \mu m$; $R_{max} = 8 \mu m$. (B) Corresponding reduced model calculation with $K_s = K_m = 10 \mu M$.

1 A) were chosen to represent the cytosolic milieu. For example, the diffusion constant for free Ca^{2+} used in this simulation ($D_c = 250 \ \mu m^2 \ s^{-1}$) is based on experimental data (Allbritton et al., 1992). We have assumed dissociation constants for endogenous buffers to be in the range of 1–10 μM (see Table 1) and chosen concentrations for total stationary ($[B_s]_T$) and total mobile ($[B_m]_T$) buffer that are consistent with the effective diffusion constant for Ca^{2+} measured in *Xenopus* cytoplasm (Allbritton et al., 1992). The association and dissociation rates of the buffers ($k_s^- = k_m^- = 10^3 \ s^{-1}$, $k_s^+ = k_m^+ = 10^2 \ \mu M^{-1} \ s^{-1}$) are compatible with measurements of relaxation times for endogenous Ca^{2+} buffers in chromaffin cells (Zhou and Neher, 1993). In agreement with theoretical arguments, we find micromolar concentrations of Ca^{2+} adjacent to the open channel (Neher, 1986) with $[Ca^{2+}]$ greater than 100 μM at distances less than 100 nm from the 5-pA source. On the other hand, at 1 ms these elevated Ca^{2+} concentrations are restricted to a region approximately 0.5–1.0 μm in radius, beyond which $[Ca^{2+}]$ approaches the background concentration of 0.1 μM. The evolution of the Ca^{2+} profile through time depends heavily on the current amplitude of the source as well as on the concentration, kinetics, and mobility of the endogenous Ca^{2+} buffers used in the full model calculation.

The effect of mobile Ca^{2+} buffers near an open Ca^{2+} channel can be observed in Fig. 1 A by comparing the free stationary buffer concentration ($[B_s]$, *dotted line*) with the free mobile buffer concentration ($[B_m]$, *long-dashed line*). At large distances from the source, the concentrations of both stationary and mobile buffers are in equilibrium with the background Ca^{2+} concentration ($[B_s] = 247.5 \ \mu M$, $[CaB_s] = 2.5 \ \mu M$, $[B_m] = 49.5 \ \mu M$, and $[CaB_m] = 0.5 \ \mu M$). Near the channel the concentrations of both free stationary and free mobile buffers decrease. But whereas the free stationary buffer concentration near the source approaches zero, the free mobile buffer concentration is approximately 6.0 μM. Even at a distance of 10 nm, where the stationary buffer is more than 99% saturated, the mobile buffer is only 83% saturated. This difference in degree of saturation is due to the ability of free mobile buffer (B_m) and mobile buffer with Ca^{2+} bound (CaB_m) to diffuse toward and away from the channel (Roberts, 1993, 1994). Although locally the sum of $[B_m]$ and $[CaB_m]$ stays constant when their diffusion constants are equal, the net effect of the diffusion of mobile buffer in these two different forms is to replace the mobile buffer with Ca^{2+} bound (CaB_m) near the source with free mobile buffer (B_m). Regardless of concentration, stationary buffer cannot influence the steady-state Ca^{2+} profile near an open channel, but only the approach to this dynamic steady state. Mobile buffer, on the other hand, can have a dramatic effect on both the time course of the Ca^{2+} profile and its steady state (Roberts, 1993, 1994).

Fig. 1 B shows the reduced model calculation corresponding to the full model calculation in Fig. 1 A. This calculation assumes instantaneous equilibration of Ca^{2+} with stationary and mobile buffer, but uses the same diffusion (D_m) and dissociation (K_s and K_m) constants as Fig. 1

A. One practical advantage of the rapid buffering approximation is that only the Ca^{2+} concentration need be explicitly calculated; for comparison, however, in Fig. 1 B we present the concentrations of the buffers calculated from the equilibrium assumption. Qualitatively and semiquantitatively, the full and reduced model calculations are remarkably similar. For example, at a distance of 0.1 μm from the source, the Ca^{2+} concentration is elevated to approximately 110 μM, and stationary buffer is 92% saturated in both the full and reduced model calculations. However, closer inspection reveals some disagreement between the two calculations. The Ca^{2+} profile has a decreased extent in the reduced model calculation, approaching the background Ca^{2+} concentration of 0.1 μM at a distance of 0.7 μm, rather than 1.0 μm, from the origin. A shift in the CaB_s and B_s profiles can be observed by noting the distance at which these two traces cross each other, i.e., the radius at which stationary buffer sites are 50% saturated. This radius is 0.27 μm in the full model and 0.29 μm in the reduced model calculation. In the case of mobile buffer, this shift is greater (0.19 μm versus 0.29 μm). In addition, near the source the free mobile buffer concentration is much lower in Fig. 1 B than in Fig. 1 A. These observations suggest that the quantitative accuracy of the rapid buffering approximation depends on the mobility of the Ca^{2+} buffers being considered.

Fig. 2 compares the reduced model calculation (*solid line* in Fig. 2 and Fig. 1 B) to the Ca^{2+} profiles of full model calculations in which the association and dissociation rate constants (k_s^+, k_m^+, k_s^-, and k_m^-) are increased while maintaining the same dissociation constants ($K_s = K_m = 10$ μM). As in Fig. 1, the Ca^{2+} profiles are shown at an elapsed time of 1 ms. The uppermost Ca^{2+} profile in Fig. 2 (*dotted line*) was calculated using the full model with relatively slow association and dissociation rate constants ($k_s^- = k_m^- = 10 \ s^{-1}$, $k_s^+ = k_m^+ = 1 \ \mu M^{-1} \ s^{-1}$). This profile differs significantly from the corresponding reduced model calculation (*solid line*). For example, at a distance of 0.6 μm from
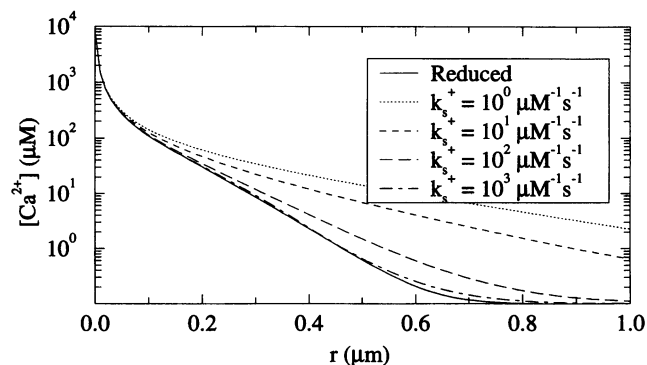

FIGURE 2 Reduced model calculation of $[Ca^{2+}]$ profile (*solid line*) in Fig. 1 B is compared to $[Ca^{2+}]$ profiles (*broken lines*) calculated using the full model with a range of association and dissociation rate constants ($k_s^+ = k_m^+ = 10^0-10^3 \ \mu M^{-1} \ s^{-1}$; $k_s^- = k_m^- = 10^1-10^4 \ s^{-1}$), varied so that $K_s = K_m = 10 \ \mu M$; other parameters are as in Fig. 1. The reduced model result approaches the full model as buffer kinetic constants are increased.

the source, there is a difference of nearly two orders of magnitude in the Ca^{2+} concentration predicted by the full and reduced models. However, as the association and dissociation rate constants used in the full model are increased, the difference between the calculated Ca^{2+} profiles diminishes. The lowermost broken trace (dot-dashed line) is a full model calculation ($k_s^- = k_m^- = 10^4$ s^{-1} and $k_s^+ = k_m^+ = 103$ μM^{-1} s^{-1}) that is nearly identical to the reduced model. Comparison of these Ca^{2+} profiles verifies that as the buffering rate constants in the full model are increased, the full model Ca^{2+} profile approaches that of the reduced model. This convergence is guaranteed by the fact that the reduced equation is derived from the full equations assuming that Ca^{2+} is always locally in equilibrium with the buffers, a condition that is satisfied when the rate constants in the full model are large. Taken together, Figs. 1 and 2 show the validity of the rapid buffering approximation near a point source for free Ca^{2+} when Ca^{2+} buffers are sufficiently fast, and that the adequacy of this approximation depends on the kinetic constants of the Ca^{2+} buffers (Wagner and Keizer, 1994).

Because the rapid buffering approximation assumes that Ca^{2+} instantaneously equilibrates with the buffers, it is tempting to conclude that the Ca^{2+} profile calculated with the reduced equation will always lie below that calculated with the full equations. For example, in Figs. 1 and 2 the reduced model underestimates the concentration of Ca^{2+} throughout the Ca^{2+} domain. This is often observed in simulations near a channel that has been open continuously (see also Fig. 3). However, we have found conditions in which the local Ca^{2+} concentration in the reduced model exceeds that in the corresponding full model calculation (cf. Fig. 7). In the case of a periodically switching source (not shown), the reduced model calculation can transiently exceed the full model calculation when the source turns off.

Although the reduced model result is always the limit of the full model calculations as buffer rates are increased, the

utility of the reduced model depends on its convergence to the full model, where buffer rate constants are plausible physiologically. Using such realistic parameters ($\sigma = 5$ pA, $K_i = 10$ μM, $k_i^+ = 10^2$ μM^{-1} s^{-1}, and $k_i^- = 10^3$ s^{-1}), Fig. 3 directly compares full and reduced model calculations while varying both the fraction of mobile to stationary buffer and the elapsed time. In all cases, total Ca^{2+} buffer ($[B_s]_T + [B_m]_T$) is 300 μM. Fig. 3 A presents full and reduced model calculations for the case of 100% stationary buffer at 1 ms. Here the difference between the Ca^{2+} profiles predicted by the reduced and full models varies greatly as a function of distance from the source. For example, there is nearly an order of magnitude difference between the Ca^{2+} concentration predicted by the reduced and full models at $r = 0.6$ μm, whereas the difference at the origin and at $r = 1.0$ μm is negligible. However, this difference between the full and reduced calculation decreases with time (cf. Fig. 3, A and B). Although at 1 ms elapsed time the difference between the two calculations is pronounced (see 0.4 $\mu m < r < 0.8$ μm), by 10 ms the full and reduced models are predicting nearly identical Ca^{2+} profiles. The mobility, concentration, and kinetic rate constants of the Ca^{2+} buffers determine the time at which this convergence occurs. The 1-ms time constant of relaxation for the stationary buffers used in this simulation is a rough lower bound to the time it takes for the reduced model to converge to the full model.

The effect of endogenous mobile Ca^{2+} buffer on the validity of the rapid buffering approximation is shown in Fig. 3, C and D, which are identical to Fig. 3, A and B, except for the replacement of 50 μM stationary buffer by 50 μM mobile buffer ($[B_s]_T = 250$ μM, $[B_m]_T = 50$ μM, and $D_m = 75$ μm^2 s^{-1}). At 1 ms, the reduced model calculation has not yet converged to the full model (Fig. 3 C), but by 10 ms the two models are giving nearly identical results (Fig. 3 D). Although in these simulations only 17% of the Ca^{2+} buffer is mobile, the manner in which the reduced model

FIGURE 3 Direct comparison of full (solid line) and reduced (dotted line) model calculations of $[Ca^{2+}]$ profile near a 5-pA source. (A) $[B_s]_T = 300$ μM; $t_0 = 1$ ms. (B) $[B_s]_T = 300$ μM; $t_0 = 10$ ms. (C) $[B_s]_T = 250$ μM; $[B_m]_T = 50$ μM; $t_0 = 1$ ms. (D) $[B_s]_T = 250$ μM; $[B_m]_T = 50$ μM; $t_0 = 10$ ms. (E) $[B_m]_T = 300$ μM; $t_0 = 1$ ms. (F) $[B_m]_T = 300$ μM; $t_0 = 10$ ms. In all cases, $k_s^- = k_m^- = 10^3$ s^{-1} and $k_s^+ = k_m^+ = 10^2$ μM^{-1} s^{-1}. All other parameters are the same as Fig. 1. In each panel, coarse-grained results ($\Delta R = 1$ μm; see text) for the full (O) and reduced ($\triangle$) model are shown at $r = 0$ μm and $r = 1$ μm.
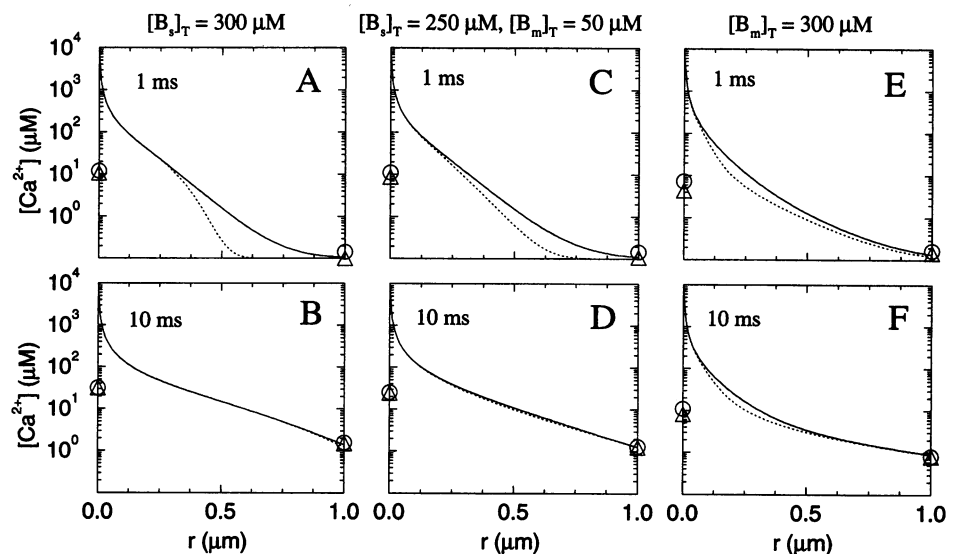
converges to the full model calculation is different from the case of 100% stationary buffer (cf. the dotted line in Fig. 3 C with the dotted line in Fig. 3 A). For example, at an elapsed time of 1 ms, the presence of mobile buffer increases the region over which the full and reduced models disagree. Furthermore, the smallest radii at which this difference is significant are closer to the source when 17% mobile buffer is included in the simulation. On the other hand, there are some radii at which the full and reduced model calculations are more similar in the presence of 17% mobile buffer than 100% stationary buffer (cf. Fig. 3, C and A, at $r = 0.6$ μm). Most importantly, the difference between the two calculations decreases with time, and by 10 ms elapsed time this convergence is largely, but not entirely, complete (cf. Fig. 3, C and D).

When the full and reduced model calculations are compared in the case of 100% mobile buffer ([B_m] = 300 μM, Fig. 3, E and F), these trends continue. The region over which the full and reduced models disagree enlarges toward the source, whereas at some radii the difference between the full and reduced model becomes less pronounced (cf. Fig. 3, E and C). And once again, the two calculations converge as the simulation time progresses. Although at 10 ms this convergence is less robust in the case of 100% mobile buffer than with 17% mobile buffer (cf. Fig. 3, F and D), agreement is still semiquantitative once the equilibration time of the buffers has elapsed.

The rapid buffering approximation permits a simple interpretation of the shape and time course of the calcium profiles in Fig. 3. According to Eq. 10, the differential fraction of free to bound Ca^{2+} (β) scales the time rate of change of [Ca^{2+}], making it slower than in the absence of buffer. This is reflected in a reduced effective diffusion coefficient for Ca^{2+} given by (Wagner and Keizer, 1994).

$$D_{eff} = \beta\left(D_c + \sum_j \gamma_j D_j\right). \tag{13}$$

Note that whether they are stationary or mobile, all buffers decrease the effective diffusion coefficient (D_{eff}) by reducing the contribution of the free diffusion constant (D_c) for Ca^{2+} by a factor of β, whereas in the case of mobile buffer, the remaining terms in D_{eff} partially compensate for this decrease. This means that the spread of Ca^{2+} from the source by diffusion is considerably slower than in the absence of buffers and will be even slower if the buffers are all stationary. In addition, the second term in Eq. 10 shows that mobile buffers act as a sink for Ca^{2+} (Wagner and Keizer, 1994) that is more effective the steeper the gradient (∇[Ca^{2+}]). These facts imply that within a few microseconds the Ca^{2+} profile falls off near the source like $\sigma_0/2\pi D_c r$, because $D_{eff} \simeq D_c$ as the buffers become saturated. At intermediate distances the sink term, which is caused by the mobile buffers carrying Ca^{2+} away, forces the Ca^{2+} profile to fall off faster in the presence than in the absence of mobile buffers. Far from the source the larger effective

diffusion coefficient for the mobile buffers means that the concentration of Ca^{2+} will be larger than for an equivalent amount of stationary buffer. All of these features are recognizable in Fig. 3.

COARSE GRAINING AND ERROR CALCULATIONS

Experimental resolution of Ca^{2+} domains is restricted by current techniques to a distance scale on the order of microns and a time scale on the order of milliseconds. Although our calculations are not restricted to this low resolution, it is important to compare the full and the reduced model calculations of Ca^{2+} domains on these coarse-grained scales. This requires averaging over space and time intervals that are appropriate to experimental resolution. We have found that averaging over space suffices to give quite good agreement between the two types of calculations, and thus we restrict our discussion to coarse-graining of space.

Because our calculations have spherical symmetry, course-grained spatial averages are given by

$$\overline{[Ca^{2+}]}(r, t) = \int_{r-\frac{\Delta R}{2}}^{r+\frac{\Delta R}{2}} [Ca^{2+}](\rho, t)\rho^2 d\rho \Big/ \int_{r-\frac{\Delta R}{2}}^{r+\frac{\Delta R}{2}} \rho^2 d\rho, \tag{14}$$

except for $r = 0$, where

$$\overline{[Ca^{2+}]}(0, t) = \frac{24}{\Delta R^3} \int_0^{\frac{\Delta R}{2}} [Ca^{2+}](\rho, t)\rho^2 d\rho. \tag{15}$$

In these equations ΔR defines the radial length scale over which [Ca^{2+}] is averaged, resulting in a coarse-grained concentration at the radial location r. Note that as r increases this definition averages over larger volumes, all of the same radial thickness. Typical results of this type of averaging using a length scale of $\Delta R = 1.0$ μm are given by the circles and triangles in Fig. 3. The circles represent the coarse-graining of the full model calculation, and the triangles represent the reduced model calculation. In the presence of either 100% stationary (Fig. 3, A and B) or 17% mobile (Fig. 3, C and D) buffer, the coarse-grained averages are in good agreement already at 1 ms. Even when all of the buffer is mobile (Fig. 3, E and F), which means that significant gradients in the concentration of occupied buffer develop (cf. Fig. 1 A), the two coarse-grained averages differ by less than a factor of 2 near the origin after only 1 ms of elapsed time.

To quantify these differences, we have calculated the magnitude of the fractional difference between the two coarse-grained calculations relative to the coarse-grained full model calculation, $E(r, t)$, using $\Delta R = 1.0$ μm. Fig. 4 plots $E(0, t)$ evaluated at the origin as a function of time for 100% stationary buffer (solid line), 17% mobile buffer (dotted line), and 100% mobile buffer (dashed line). The parameters used here are identical to those in Fig. 3 and give an equilibration time for the buffers on the order of 1 ms. In
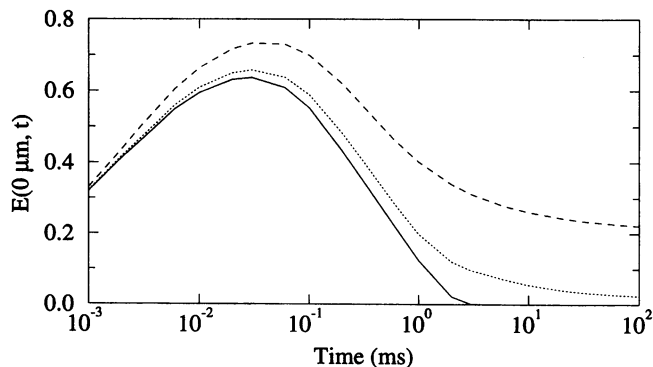
FIGURE 4 $E(0, t)$, the coarse-grained ($\Delta R = 1 \ \mu m$) error of the rapid buffering approximation evaluated at $r = 0$, is shown as a function of time for the case of stationary buffer only ([B_s]$_T$ = 300 μM; *solid line*), a mix of stationary and mobile buffer ([B_s]$_T$ = 250 μM; [B_m]$_T$ = 50 μM; *dotted line*), and 100% mobile buffer ([B_m]$_T$ = 300 μM; *dashed line*). Other parameters are the same as in Fig. 1.

all three cases, the error in the rapid buffering approximation is large shortly after the channel opens, but decreases considerably after several milliseconds. In the case of 100% stationary buffer, the error falls below 0.1 after 1 ms and is vanishingly small after 10 ms. In the case of 17% mobile buffer, these numbers are 0.2 and 0.05, respectively. This difference is due to the sink for Ca^{2+} produced by mobile buffers (i.e., the second term in Eq. 10) as they move in to replace buffer that is bound to Ca^{2+}. This process results in steeper Ca^{2+} gradients (compare Fig. 3, F and B), and, consequently, more time must pass before the condition of validity of the rapid buffering approximation given in Eq. 12 is satisfied. Although 100% mobile buffer is not realistic physiologically, the top trace in Fig. 4 emphasizes that the length of time required for the coarse-grained error to vanish depends on the quantity of mobile buffer and suggests

that the rapid buffering approximation is better when only moderate concentrations of mobile buffer are present.

Fig. 5 quantifies the validity of the rapid buffering approximation over a wide range of buffer rate constants. Fig. 5, A and B, presents $E(0, t)$ at 1.0 and 10 ms, respectively, for stationary buffer dissociation constants (K_s) of 1 μM (*dotted line*) and 10 μM (*solid line*) and a variety of association rate constants (k_s^+). Fig. 5, C and D, gives similar results for a mixture of stationary and mobile buffers with identical kinetics ($k_s^+ = k_m^+$, $k_s^- = k_m^-$). To interpret these results, recall that for a given dissociation constant (K_i), increasing the association rate constant (k_i^+) implies a proportional increase in k_i^-, which together result in a greater equilibration rate for the buffers. Thus each panel in Fig. 5 shows that error greatly decreases as the equilibration rate of the buffers increases. Although over time error decreases more slowly in the case of a mixture of stationary and mobile buffer than in the case of 100% stationary buffer (compare Fig. 5, D and B), in both cases the coarse-grained error decreases as a function of time, regardless of buffer parameters (compare Fig. 5 B to 5 A and 5 D to 5 C). Within 10 ms after the source activates, the error is less than 0.1 for stationary buffers with association rates greater than 10 $\mu M^{-1} s^{-1}$, and in this regime error is approaching 0.1 for the mixture of stationary and mobile buffers.

Fig. 5 also shows that error is generally greater in the case of high-affinity buffers (*dotted lines*) than low-affinity buffers (*solid lines*). To understand this recall that the dissociation rate constant for Ca^{2+} from the buffers is given by $k_i^- = k_i^+ K_i$. Thus, in each panel, the dissociation constant (k_i^-) of the solid curve is a factor of 10 larger than that of the corresponding dotted curve. As the equality in Eq. 12 shows, this increased dissociation constant considerably lengthens the equilibration time of the buffers unless the association rate constant is comparatively large. In Fig. 5 D,
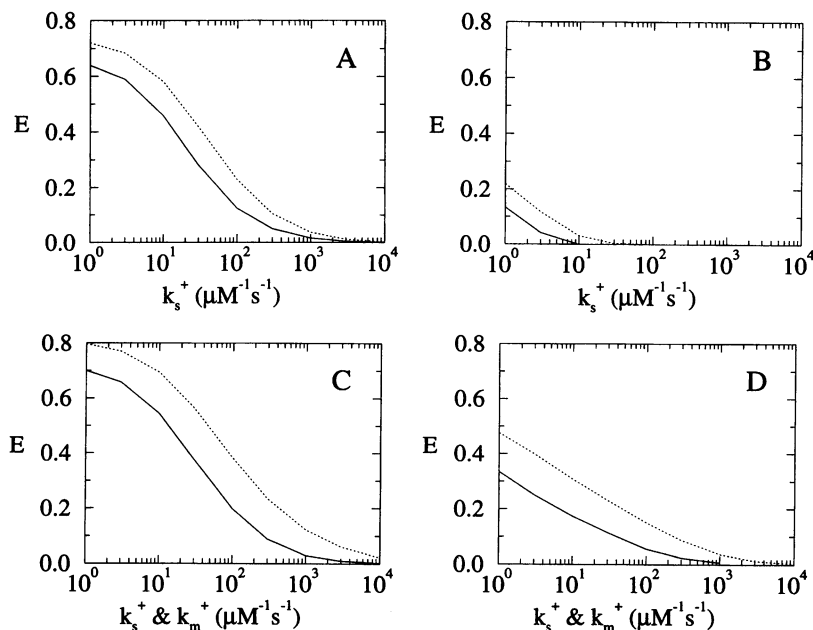

FIGURE 5 $E(0, 1 \text{ ms})$ and $E(0, 10 \text{ ms})$ for $\Delta R = 1$ μm calculated as a function of buffer parameters. In each graph the error decreases as the association (k_i^+) and dissociation (k_i^-) rate constants are increased proportionately. The solid line represents $K_i = 10 \ \mu M$, and the dashed line represents $K_i = 1 \ \mu M$. (A) [B_s]$_T$ = 300 μM; $t_0 = 1$ ms. (B) [B_s]$_T$ = 300 μM; $t_0 = 10$ ms. (C) [B_s]$_T$ = 250 μM; [B_m]$_T$ = 50 μM; $t_0 = 1$ ms. (D) [B_s]$_T$ = 250 μM; [B_m]$_T$ = 50 μM; $t_0 = 10$ ms.

for example, for an association rate constant of $k_i^+ = 10^2$ $\mu M^{-1} s^{-1}$, the dotted curve represents a dissociation rate of $k_i^- = 10^2 s^{-1}$, whereas the solid curve represents $k_i^- = 10^3$ s^{-1}. These values of k_i^+ and k_i^- result in an equilibration time on the order of a millisecond for both curves, with the dotted curve ($K_i = 1$ μM) being about a factor of 2 slower than the solid curve ($K_i = 10$ μM).

The validity of the rapid buffering approximation also depends on the current amplitude of the source. This is shown in Fig. 6, where $E(0, t)$ is plotted as a function of the unitary current at 1 ms (*solid line*) and 10 ms (*dotted line*). Both stationary and mobile buffers are included in the calculation with parameters identical to Figs. 1, 3 C, and 3 D. $E(0, 10$ ms) is lower than $E(0, 1$ ms) for all source amplitudes greater than 0.1 pA. In addition, at both times the error is greatest at intermediate source amplitudes (near 0.5 or 0.9 pA). At low source amplitudes, the coarse-grained Ca^{2+} concentration of both the full and reduced models is near background and the error is consequently low. When the current is high, error is minimized because buffers near the source are saturated.

EFFECT OF EXOGENOUS BUFFERS

Because the rapid buffering approximation is a good one near a 5-pA source, it makes sense to use the reduced model to describe the IP_3-mediated Ca^{2+} release events known as Ca^{2+} "puffs" (Yao et al., 1995). In the simulations shown in Fig. 7, the source corresponds to a cluster of 10 open IP_3 receptors, each with a unitary current amplitude of 0.5 pA (Bezprozvanny and Ehrlich, 1994). This Ca^{2+} "release site" is instantaneously activated at $t = 0$ and remains active for 50 ms, the duration of an average Ca^{2+} puff event observed in the immature *Xenopus* oocyte (Yao et al., 1995), at which time it is instantaneously inactivated. In Fig. 7 A, a simulated Ca^{2+} puff is shown while the source is active at 1, 10, and 50 ms. Fig. 7 B shows the Ca^{2+} profile again at 50 ms as well as the profile 1, 10, and 50 ms after the source inactivates. Beginning with the 10-ms Ca^{2+} profile, calcu-

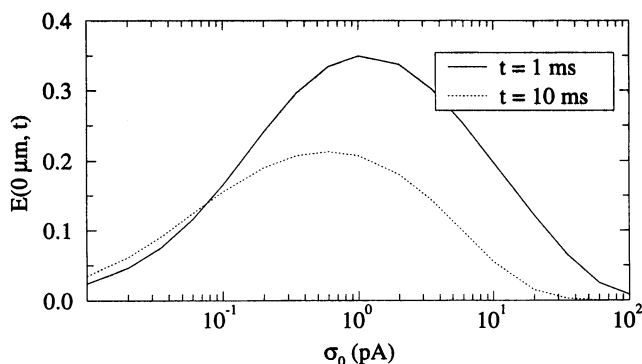lations using the full and reduced model are nearly identical, even after the source inactivates.

We have also used the full and reduced models to examine the effect of Ca^{2+} indicator dye on the spatiotemporal profile of a simulated puff. The "puff" in Fig. 7, C and D, is identical with that in Fig. 7, A and B, except for the addition of 50 μM exogenous mobile Ca^{2+} buffer with parameters ($k_e^- = 200$ $\mu M^{-1} s^{-1}$, and $k_e^+ = 600$ s^{-1}, K_e of 0.3 μM) chosen to approximate Ca^{2+} Green-1 (see Table 1), a high-affinity Ca^{2+} indicator dye that has been used to image Ca^{2+} puffs (Yao et al., 1995). Comparison of these simulations shows that Ca^{2+} Green-1 restricts the maximum size of the Ca^{2+} domain formed during the puff event. For example, in the absence of exogenous buffer, the radius of the region above 1 μM at 50 ms is 1.8 μm (Fig. 7 A), but in the presence of Ca^{2+} Green-1, this radius decreases to 1.0 μm. Another effect of the indicator dye is apparent after the source has been inactivated. Comparison of the bottommost traces of Fig. 7, B and D, reveals that the presence of high-affinity exogenous mobile buffer facilitates clearance of Ca^{2+}. Indeed, 50 ms after the puff has inactivated (bottommost trace in Fig. 7, D and F), there is an order of magnitude difference between the Ca^{2+} concentration predicted in the presence and absence of Ca^{2+} indicator dye. Note that although the effect of the Ca^{2+} indicator dye is large, the consequence of its addition is predicted by the reduced model as well as the full model. In spite of the low dissociation constant for Ca^{2+} Green-1 ($K_e = 0.3$ μM), the rapid buffering approximation is excellent, given the moderate concentration of exogenous mobile buffer present in the simulation.

A reduced model calculation is a theoretical approximation to the "correct result," i.e., the full model calculation. The rapid buffering approximation, however, is different from applying the assumption of equilibrium to "back-calculate" [Ca^{2+}] from an experimentally obtained fluorescence signal (Grynkiewicz et al., 1985). The inadequacy of "back-calculation" can be seen in Fig. 7, E and F, where the full model calculation (same as Fig. 7, C and D) is compared to the "back-calculated" Ca^{2+} profiles derived from the exogenous, bound Ca^{2+} indicator (CaB_e) profile of the full model, assuming that Ca^{2+} is in equilibrium with dye at each point in space. As can be seen in Fig. 7, E and F, these back-calculated Ca^{2+} profiles underestimate the actual [Ca^{2+}], especially when the source is on. This discrepancy can be attributed to the fact that the indicator dye remains out of equilibrium with Ca^{2+} throughout the duration of the puff. Although the rapid buffering approximation and back-calculation utilize the assumption of equilibrium, the rapid buffering approximation gives results closer to the full model than the back-calculated Ca^{2+} profile. It is interesting to note that back-calculation from the concentration of bound dye improves considerably when the dye is immobilized (not shown), suggesting that fluorescent dyes conjugated to macromolecules such as dextran should provide more accurate estimates of punctate [Ca^{2+}]. These observations imply that when calculations of localized Ca^{2+}

FIGURE 6 $E(0, 1$ ms) and $E(0, 10$ ms) for $\Delta R = 1$ μm calculated as a function of source amplitude (0.01–100 pA); other parameters are as in Fig. 1.

FIGURE 7 Full model (*solid lines*), reduced model (*dotted lines*), and back-calculated (*dot-dashed lines*) simulations of Ca^{2+} puffs in the absence (*A, B*) or presence (*C–F*) of exogenous Ca^{2+} indicator dye. A 5-pA source representing a single Ca^{2+} release site is turned on at $t = 0$ and turned off at $t = 50$ ms. (*A, C*, and *E*) Ca^{2+} profiles at 1, 10, and 50 ms. (*B, D*, and *F*) Ca^{2+} profiles at 50, 51, 60, and 100 ms. (*A, B*) $[B_s]_T = 250$ μM; $[B_m]_T = 50$ μM; $k_s^- = k_m^- = 10^3$ s^{-1}; $k_s^+ = k_m^+ = 10^2$ μM^{-1} s^{-1}. (*C, D*) Same as *A* and *B*, with exogenous dye parameters: $[B_e]_T = 50$ μM; $k_e^- = 200$ s^{-1}; $k_e^+ = 600$ μM^{-1} s^{-1}; $D_e = 75$ μm^2 s^{-1}. (*E, F*) Dot-dashed lines are the $[Ca^{2+}]$ profile back-calculated from the full model calculation of Ca^{2+} bound to indicator dye, i.e., the $[Ca^{2+}]$ that would be in equilibrium with the $[CaB_e]$ profile (not shown) of *C* and *D*. For comparison, the $[Ca^{2+}]$ profile as calculated by the full model (*solid lines*) is shown again.
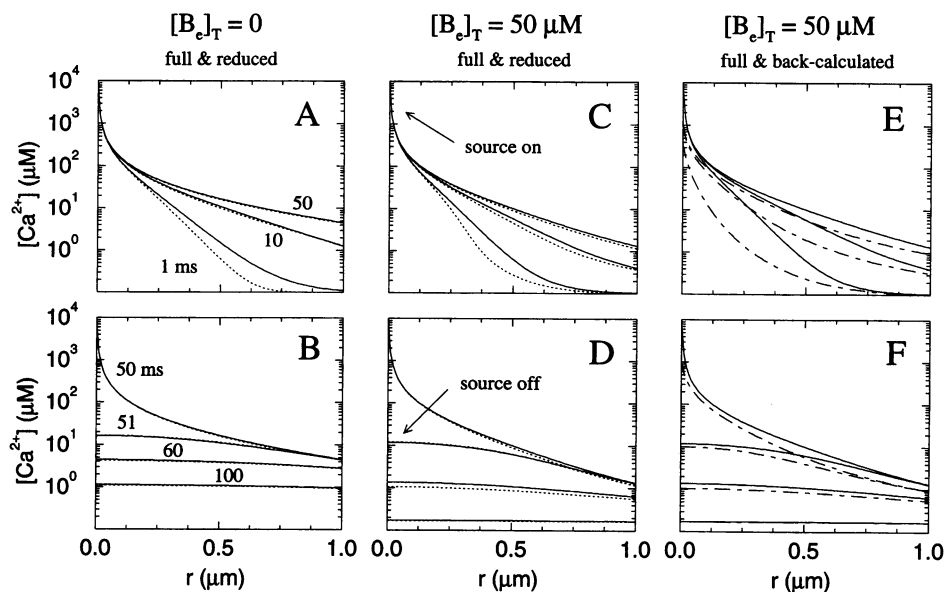
domains are related to experimental results, it is preferable to compare the theoretical CaB_e profile directly to the raw fluorescence measurement.

Fig. 8 shows a time series of coarse-grained full and reduced model calculations, both with and without the indicator dye Ca^{2+} Green-1. This figure is derived from calculations like those in Fig. 7 and includes a time series of the coarse-grained, back-calculated Ca^{2+} profile. Comparison of the full model calculations (*solid lines*) shows that the indicator dye decreases the coarse-grained (i.e., experimentally observable) Ca^{2+} concentration throughout the duration of the puff event, especially when the source is active. In addition, this figure shows that given the resolution of current Ca^{2+} measurements ($\Delta R = 1$ μm), the maximum error of the rapid buffering approximation during the time course of the puff is approximately 6%, less than
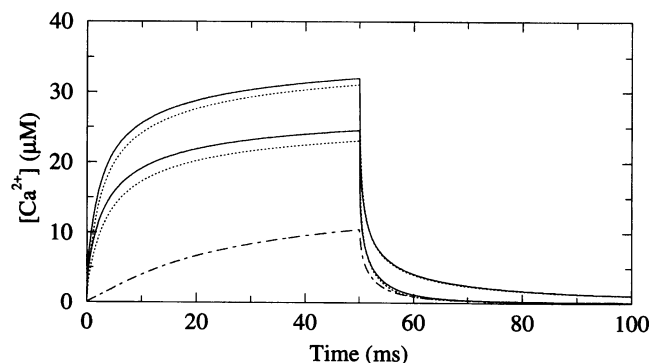

FIGURE 8 $[Ca^{2+}](0, t)$ coarse grained with $\Delta R = 1$ μm for the simulations presented in Fig. 7. The uppermost reduced (*dotted line*) and full (*solid line*) model calculations do not include Ca^{2+} indicator dye and correspond to Fig. 7, *A* and *B*. The middle two traces include exogenous Ca^{2+} dye and correspond to Fig. 7, *C* and *D*. The lowermost, dot-dashed trace is the back-calculated Ca^{2+} profile corresponding to Fig. 7, *E* and *F*.

the attenuation of the Ca^{2+} profile caused by the indicator dye itself (23%), and quite small compared to the error accrued through back-calculation of Ca^{2+} concentrations from fluorescence data (67%).

We have also investigated the validity of the rapid buffering approximation in simulations of the Ca^{2+} domain near an open channel with a unitary current of 0.1 pA. This 50-fold reduction in source strength compared to Fig. 1 is meant to simulate an isolated L-type Ca^{2+} channel, whereas the other parameters used here are identical to those of Fig. 1. The top two traces in Fig. 9 *A* show the full and reduced model calculation of the Ca^{2+} domain at high spatial resolution. Even on this finer spatial scale, the reduced and full model calculations are in qualitative agreement (for quantitative comparison of the coarse-grained error, see Fig. 6).

Although the rapid buffering approximation works well at physiologically realistic concentrations of buffers, it is not a good approximation when extremely high concentrations of exogenous buffers are present. This is shown in the bottom two traces in Fig. 9 *A*, which are identical to the top two traces, except that 1 mM exogenous buffer ($k_e^- = 90$ s^{-1} and $k_e^+ = 600$ μM^{-1} s^{-1}), chosen to approximate BAPTA (Stern, 1992; Zweifach and Lewis, 1995; see Table 1), is included in the simulation. Whereas the full model calculation correctly predicts the restricted Ca^{2+} domain formed in the presence of 1 mM BAPTA, the reduced model severely underestimates the Ca^{2+} concentration throughout the region of interest. Millimolar concentrations of exogenous mobile buffer dramatically increase the Ca^{2+} gradient near the source; consequently, the rapid buffering approximation fails in spite of the fact that BAPTA is a relatively fast Ca^{2+} buffer (cf. Eq. 12).

The reason for this can be seen by comparing the rapid buffering approximation with an analytical expression presented by Neher (1986) for the steady-state free Ca^{2+} con-
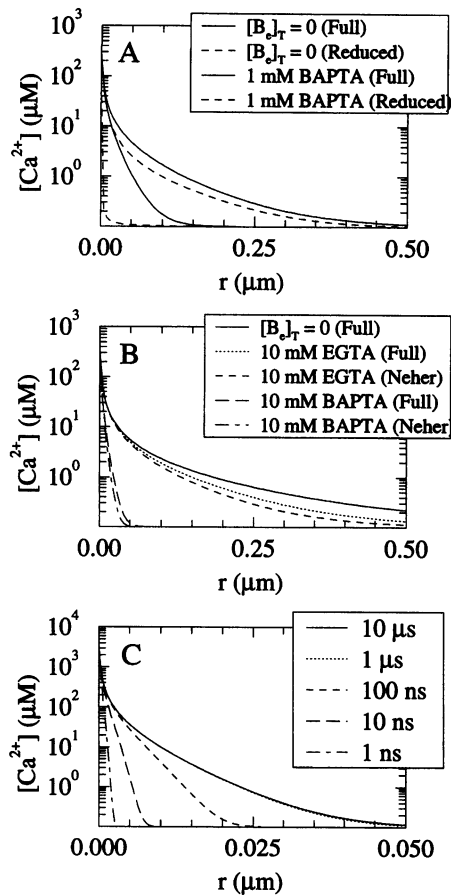
FIGURE 9 Full model calculations of the microscopic Ca^{2+} domain hypothesized to form near an open Ca^{2+} channel with a conductance of 0.1 pA. Parameters are the same as in Fig. 1 *A*, except $\Delta t = 2.5 \times 10^{-8}$ s, $\Delta r = 5$ nm, and $R_{max} = 4$ μm. (*A*) Full (*solid line*) and reduced (*dashed line*) model calculations of the Ca^{2+} domain in the presence (*bottom two traces*) and absence (*top two traces*) of 1 mM BAPTA. Parameters used for BAPTA are $k_e^- = 90$ s^{-1}, $k_e^+ = 600$ μM^{-1} s^{-1}, $K_e = 0.15$ μM, and $t_0 = 1$ ms. All other parameters are the same as in Fig. 1. (*B*) Ca^{2+} domain predicted in the presence of 10 mM EGTA (*dotted line*), 10 mM BAPTA (*long-dashed line*), and no exogenous buffer (*solid line*). Parameters used for EGTA are $k_e^- = 0.225$ s^{-1}, $k_e^+ = 1.5$ μM^{-1} s^{-1}, $K_e = 0.15$ μM, and $t_0 = 10$ ms. Other parameters are as in *A*, except that endogenous buffers were not included in the BAPTA and EGTA simulations, so that they may be directly compared to the corresponding steady-state approximations (*short-dashed* and *dot-dashed lines*) given by Eq. 16. (*C*) The Ca^{2+} domain in the case of 10 mM BAPTA at $t_0 = 0.001, 0.01, 0.1, 1,$ and 10 μs. Other parameters are as in *A*.

centration ($[Ca^{2+}]_{ss}$) near a single channel. That expression, which is valid for small source amplitude and unsaturatable (high concentrations of) mobile buffer, is

$$[Ca^{2+}]_{ss}(r) \approx \frac{\sigma_0}{2\pi D_c r} e^{-r/\lambda}, \qquad (16)$$

where

$$\lambda = \sqrt{\frac{D_c}{k_e^+ [B_e]_T}}. \qquad (17)$$

The conditions for the validity of Eq. 16 are precisely those for which the rapid buffering approximation is least valid. Indeed, at high concentrations the condition for the validity of the rapid buffering approximation in Eq. 12, as applied to the exogenous buffer, becomes

$$\tau_e \approx \frac{1}{k_e^+ [B_e]_T} \ll \frac{L^2}{D_c}, \qquad (18)$$

which is not satisfied when $\lambda = L$, the length characteristic of the spatial profile of Ca^{2+}. Thus the rapid buffering approximation breaks down because of the steep gradients that occur at high concentrations of exogenous mobile buffer—making it necessary to use the full equations.

Fig. 9 *B* presents full model calculations of the Ca^{2+} domain formed near a 0.1-pA source in the presence of 10 mM EGTA (*short dashed line*), 10 mM BAPTA (*long dashed line*), and no exogenous buffer (*solid line*). Parameters were chosen to approximate a slow, EGTA-like buffer ($k_e^- = 0.225$ s^{-1} and $k_e^+ = 1.5$ μM^{-1} s^{-1}; Stern, 1992; Zweifach and Lewis, 1995; see Table 1) with the same dissociation constant as BAPTA ($K_e = 0.15$ μM). Comparison between the calculations in Fig. 9 *B* shows that the Ca^{2+} domain is greatly restricted in the presence of 10 mM BAPTA, but only slightly restricted by 10 mM EGTA (Stern, 1992). In addition, for both EGTA ($\lambda = 129$ nm) and BAPTA ($\lambda = 6.5$ nm), Neher's approximation of the steady-state Ca^{2+} profile (*dotted lines*) only slightly underestimates the extent of the Ca^{2+} domain. Our calculations also agree with previous calculations showing that Ca^{2+} domains form extremely rapidly (Fogelson and Zucker, 1985). Fig. 9 *C* shows a Ca^{2+} domain in the presence of 10 mM BAPTA at 0.001, 0.01, 0.1, 1, and 10 μs, with even greater spatial resolution than Fig. 9 *A*. The fact that the 10-μs profile is barely distinguishable from the 1-μs profile shows that a dynamic steady state in Ca^{2+} concentration is achieved 1 μs after the channel activates.

DISCUSSION

Our simulations show that the rapid buffering approximation provides reasonable estimates of Ca^{2+} concentrations near open Ca^{2+} channels on time scales that are comparable to the equilibration times for Ca^{2+} buffers. For endogenous buffers with representative equilibration times of a few milliseconds, this means that Ca^{2+} domains calculated with the rapid buffering approximation are correct semiquantitatively, even on a distance scale of a micron within a millisecond or so after a release site or channel has activated, whereas after 10 ms the rapid buffering approximation is nearly exact on this distance scale. We have verified this for moderate total buffer concentrations (300 μM) that appear to be representative of the cytosol in a number of cell types. According to the results in Figs. 3 and 4, the rapid buffering approximation is better for stationary buffers or stationary buffers in combination with modest concentrations of mobile buffers, in which case the errors in the space-averaged

(coarse-grained) $[Ca^{2+}]$ nearest the channel fall below 10% when the equilibration time of the buffers is exceeded.

These coarse-grained errors in reduced model calculations adjacent to an open channel depend significantly on the single-channel current. For a fixed concentration of total buffer, the rapid buffering approximation is better at either low or high values of unitary current, the latter because the buffer quickly saturates near the channel. Fig. 6 illustrates, however, that even for coarse-grained measurements one must wait for the order of the equilibration times of the buffer to reach errors of less than 10%. Our simulations of the disappearance of Ca^{2+} domains after a channel closes show that the rapid buffering approximation is quite good, as long as the channel stays open longer than the equilibration time. This remains true even in the presence of small amounts of exogenous buffer, typical of those used in fluorescence measurements.

It is not necessarily true, however, that one can "back-calculate" accurate instantaneous Ca^{2+} profiles from a knowledge of the fluorescence of exogenous dyes using the buffer dissociation constant. Indeed, Figs. 7 E, 7 F, and 8 show for both open and closed channels that the Ca^{2+} concentrations calculated in this fashion for a mobile dye fall well below those calculated via the full differential equations. Although the accuracy of this procedure improves for immobile dyes, in the presence of large, nonstationary Ca^{2+} gradients the equilibrium condition generally does not provide an accurate instantaneous relationship between measured dye-bound Ca^{2+} and Ca^{2+} concentrations. Indeed, the condition of equilibrium is strictly consistent only when applied within the context of the kinetic equations, i.e., as done in the rapid buffering approximation. This is an important caveat, because back-calculation is customarily used to estimate Ca^{2+} concentrations in fluorescence experiments.

At high concentrations of exogenous mobile buffers (10 mM), whether fast equilibrating like BAPTA or slow like EGTA, we have found that the rapid buffering approximation does not yield accurate Ca^{2+} profiles. These high buffer concentrations have been employed experimentally to manipulate the size of Ca^{2+} domains hypothesized to form near open Ca^{2+} channels (Zweifach and Lewis, 1995). In this parameter regime, the rapid buffering approximation is no longer valid. However, we have shown using the full model that Neher's equation (Eq. 16), which has been used to interpret such measurements, is a good approximation to the steady-state Ca^{2+} profile under these conditions.

When can the rapid buffering approximation be used for calculating time-dependent Ca^{2+} domains? The inequality in Eq. 12 provides the basic criterion for assessing the validity of this approximation. Whether this inequality holds depends on buffer equilibration times, the unitary current of the Ca^{2+} channel, the amount of mobile buffers, and the resolution required. Table 1, which lists properties of several known mobile and stationary endogenous buffers, can be used to estimate buffer properties when buffer concentrations are known. In saccular

hair cells, for example, calbindin-D_{28K} is thought to exist in millimolar concentrations (Roberts, 1993, 1994), and using Eq. 12 we estimate an equilibration time of 0.5 ms. However, because calbindin-D_{28K} is mobile ($D \simeq 30$ $\mu m^2 s^{-1}$; see Table 1) and is present at such high concentrations, the rapid buffering approximation breaks down near a point source for the same reason that it does for millimolar concentrations of BAPTA (cf. Eq. 18). Even for equilibration times on the order of milliseconds, moderate concentrations of mobile buffer produce Ca^{2+} gradients that are too large for the rapid buffering approximation on the millisecond time scale, whereas if less time resolution is required, then the approximation may be satisfactory. Similarly, larger unitary currents produce larger gradients, and one must wait longer for the rapid buffering approximation to be valid. On the other hand, the rapid buffering approximation produces good semiquantitative agreement for what are thought to be typical cytosolic buffer concentrations in Xenopus oocytes (Allbritton et al., 1992; Wagner and Keizer, 1994), cardiac myocytes (Berlin et al., 1994), gonadotrophs (Tse et al., 1994), and chromaffin cells (Zhou and Neher, 1993). Thus the rapid buffering approximation should prove useful for understanding time-dependent Ca^{2+} profiles in the cytosol and for estimating the properties of Ca^{2+} "puffs" (Parker and Yao, 1991; Yao et al., 1995) and "sparks" (Cheng et al., 1993). Work along these lines is currently in progress.

APPENDIX: NUMERICAL SCHEME

The Laplacian operator simplifies in the case of spherical symmetry to

$$\nabla^2 = \frac{1}{r^2}\frac{\partial}{\partial r}\left(r^2\frac{\partial}{\partial r}\right) = \frac{\partial^2}{\partial r^2} + \frac{2}{r}\frac{\partial}{\partial r}, \qquad (19)$$

the limit of which as r approaches zero can be shown by L'Hôpital's rule to be $3\partial^2/\partial r^2$ (Smith, 1985; Crank, 1975). Thus we can write

$$L(U_0^n) = \frac{3}{(\Delta r)^2}[2U_1^n - 2U_0^n] \qquad (20)$$

and

$$L(U_i^n) = \frac{1}{r_i^2(\Delta r)^2}[r_{i+1/2}^2(U_{i+1}^n - U_i^n) - r_{i-1/2}^2(U_i^n - U_{i-1}^n)] \qquad (21)$$

for $i > 0$, where U_i^n is an approximation to the function $u(r_i, t_n)$, u represents any of the species in Eqs. 2–5, $r_i = i\Delta r$, $t_n = n\Delta t$, $L(U_i^n)$ is the approximation to the Laplacian at the point (r_i, t_n), and we have used the boundary condition $(\partial u/\partial r)|_{r=0} = 0$ in its discretized form, $U_{-1}^n = U_1^n$ (Smith, 1985). Using Eqs. 20 and 21, an explicit numerical scheme for the full model that is second-order accurate in space and first-order accurate in time is given by

$$\frac{U_i^{n+1} - U_i^n}{\Delta t} = D_u L(U_i^n) + RXN(U_i^n), \qquad (22)$$

where D_u is the diffusion constant for species u; $RXN(U_i^n)$ denotes the contribution of the appropriate reaction terms in Eqs. 2–5; $L([CaB_s]_i^n)$ is

always zero; and $[B_s]$ is given by Eq. 6. Writing C_i^n for the approximation to $[Ca^{2+}]$ at the point (r_i, t_n), an explicit numerical scheme for the reduced model that is second-order accurate in space and first-order accurate in time is given by

$$\frac{C_i^{n+1} - C_i^n}{\Delta t} = \beta_i^n (L(F_i^n) + \sigma \delta_{i0}), \qquad (23)$$

where

$$\beta_i^n = \left(1 + \frac{K_s[B_s]_T}{(K_s + C_i^n)^2} + \sum_j \frac{K_j[B_j]_T}{(K_j + C_i^n)^2}\right)^{-1}, \qquad (24)$$

$$F_i^n = D_c C_i^n + \sum_j D_j \frac{[B_j]_T C_i^n}{K_j + C_i^n}, \qquad (25)$$

j = m or e; and δ_{i0}, the Kronecker delta, is zero except at the origin. The rate of change in Ca^{2+} concentration at the origin due to the presence of the source (σ), which appears explicitly in Eq. 23 and implicitly in Eq. 22, depends, of course, on the source strength, i.e.,

$$\sigma_0 = \frac{i_{ca}}{2F}, \qquad (26)$$

where i_{ca} is the current amplitude of the source (adjusted by a factor of 2), and F is Faraday's constant ($F = 9.648 \times 10^4$ coul mol^{-1}). Using Eq. 26 it can be seen that $i_{ca} = 1$ pA corresponds to $\sigma_0 \approx 5.182 \times 10^{-18}$ mol s^{-1}. Because $[Ca^{2+}]_0^n$ represents the average Ca^{2+} concentration over a sphere with radius $\Delta r/2$ and a volume (V) of $\pi \Delta r^3/6$, the rate of change in $[Ca^{2+}]$ at the origin due to the presence of the source is

$$\sigma = \frac{\sigma_0}{V} = \frac{6i_{ca}^*(5.182 \times 10^3 \ \mu M \ s^{-1})}{\pi (\Delta r^*)^3} \qquad (27)$$

where i_{ca}^* is the source strength measured in picoamps, and Δr^* is the spatial step measured in micrometers.

Calculations were performed on a 100-MHz Silicon Graphics Indigo workstation. Run time for the 1-ms simulation of the full model in Fig. 1 A was 38 min (800 spatial mesh points, 10^5 time steps). The computational labor per time step for the reduced model is 65% that of the full model. In addition, the explicit numerical scheme for the reduced model allows time steps that are an order of magnitude or more greater than those possible with the full model. This efficiency of the reduced model compared to the full model becomes even more significant in multidimensional calculations and when implicit numerical schemes are employed.

REFERENCES

Allbritton, N. L., T. Meyer, and L. Stryer. 1992. Range of messenger action of Ca^{2+} ion and inositol 1,4,5-trisphosphate. Science. 258:1812–1815.

Baimbridge, K. G., M. R. Celio, and J. H. Rogers. 1992. Ca^{2+}-binding proteins in the nervous system. Trends Neurosci. 15:303–308.

Berlin, J. R., J. W. M. Bassani, and D. M. Bers. 1994. Intrinsic cytosolic Ca^{2+} buffering properties of single rat cardiac myocytes. Biophys. J. 67:1775–1787.

Bezprozvanny, I., and B. E. Ehrlich. 1994. IP$_3$-gated Ca^{2+} channels from cerebellum—conduction properties for divalent cations and regulation by intraluminal Ca^{2+}. J. Gen. Physiol. 104:821–856.

Blatter, L. A., and W. G. Wier. 1990. Intracellular diffusion, binding, and compartmentalization of fluorescent Ca^{2+} indicators indo-1 and fura-2. Biophys. J. 58:1491–1499.

Blumenfeld, H., L. Zablow, and B. Sabatini. 1992. Evaluation of cellular mechanisms for modulation of Ca^{2+} transients using a mathematical model of fura-2 Ca^{2+} imaging in Aplysia sensory neurons. Biophys. J. 63:1146–1164.

Cannell, M. B., H. Cheng, and W. J. Lederer. 1994. Spatial non-uniformities in $[Ca^{2+}]_i$ during excitation-contraction coupling in cardiac myocytes. Biophys. J. 67:1942–1956.

Cannell, M. B., H. Cheng, and W. J. Lederer. 1995. The control of Ca^{2+} release in heart muscle. Science. 268:1045–1049.

Carslaw, H. S., and J. C. Jaeger. 1959. Conduction of Heat in Solids, 2nd ed. Clarendon Press, Oxford.

Cheng, H., W. J. Lederer, and M. B. Cannell. 1993. Calcium sparks: elementary events underlying excitation-contraction coupling in heart muscle. Science. 262:740–744.

Crank, J. 1975. The Mathematics of Diffusion, 2nd ed. Clarendon Press, Oxford.

de Leon, M., Y. Wang, L. Jones, E. Perez-Reyes, X. Wei, T. W. Soong, T. P. Snutch, and D. T. Yue. 1995. Essential Ca^{2+}-binding motif for Ca^{2+}-sensitive inactivation of L-type Ca^{2+} channels. Science. 270:1502–1506.

Eberhard, M., and P. Erne. 1991. Calcium binding to fluorescent calcium indicators: calcium green, calcium orange and calcium crimson. Biochem. Biophys. Res. Commun. 180:209–215.

Eckert, R., and J. E. Chad. 1984. Inactivation of Ca^{2+} channels. Biophys. Mol. Biol. 44:215–267.

Falke, J. J., S. K. Drake, A. L. Hazard, and O. B. Peersen. 1994. Molecular tuning of ion binding to Ca^{2+} signaling proteins. Q. Rev. Biophys. 27:219–290.

Fogelson, A., and R. Zucker. 1985. Presynaptic Ca^{2+} diffusion from various arrays of single channels. Biophys. J. 48:1003–1017.

Grynkiewicz, G., M. Poenie, and R. Y. Tsien. 1985. A new generation of Ca^{2+} indicators with greatly improved fluorescence properties. J. Biol. Chem. 260:3440–3450.

Heinemann, C., R. H. Chow, E. Neher, and R. Zucker. 1994. Kinetics of the secretory response in bovine chromaffin cells following flash photolysis of caged Ca^{2+}. Biophys. J. 67:2546–2557.

Heizmann, C. W., and W. Hunziker. 1991. Intracellular Ca^{2+}-binding proteins: more sites than insights. Trends Biochem. Sci. 16:98–103.

Jafri, M. S., and J. Keizer. 1995. On the roles of Ca^{2+} diffusion, Ca^{2+} buffers, and the endoplasmic reticulum in IP$_3$-induced Ca^{2+} waves. Biophys. J. 69:2139–2153.

Kao, J. P. Y. 1994. Practical aspects of measuring $[Ca^{2+}]$ with fluorescent indicators. Methods Cell Biol. 40:155–181.

Koster, H. P. G., A. Hartog, C. H. Van Os, and R. J. M. Bindels. 1995. Calbindin-D28K facilitates cytosolic Ca^{2+} diffusion without interfering with Ca^{2+} signalling. Cell Calcium. 18:187–196.

Llinás, R., M. Sugimori, and R. B. Silver. 1992. Microdomains of high Ca^{2+} concentration in a presynaptic terminal. Science. 256:677–679.

Neher, E. 1986. Concentration profiles of intracellular Ca^{2+} in the presence of diffusible chelator. Exp. Brain Res. Ser. 14:80–96.

Neher, E., and G. Augustine. 1992. Calcium gradients and buffers in bovine chromaffin cells. J. Physiol. (Lond.). 450:273–301.

Nowycky, M. C., and M. J. Pinter. 1993. Time courses of Ca^{2+} and Ca^{2+}-bound buffers following Ca^{2+} influx in a model cell. Biophys. J. 64:77–91.

Parker, I., and Y. Yao. 1991. Regenerative release of Ca^{2+} from functionally discrete subcellular stores by inositol trisphosphate. Proc. R. Soc. Lond. B Biol. 246:269–274.

Pethig, R., M. Kuhn, R. Payne, E. Adler, T.-H. Chen, and L. F. Jaffe. 1989. On the dissociation constants of BAPTA-type Ca^{2+} buffers. Cell Calcium. 10:491–498.

Post, J. A., and G. A. Langer. 1992. Sarcolemmal Ca^{2+} binding sites in heart. I. Molecular origin in "gas-dissected" sarcolemma. J. Membr. Biol. 129:49–57.

Roberts, W. M. 1993. Spatial Ca^{2+} buffering in saccular hair cells. Nature. 363:74–76.

Roberts, W. M. 1994. Localization of Ca^{2+} signals by a mobile Ca^{2+} buffer in frog saccular hair cells. *J. Neurosci.* 14:3246–3262.

Roberts, W. M., R. A. Jacobs, and A. J. Hudspeth. 1990. Colocalization of ion channels involved in frequency selectivity and synaptic transmission at presynaptic active zones of hair cells. *J. Neurosci.* 10:3664–3684.

Sherman, A., J. Keizer, and J. Rinzel. 1990. Domain theory for Ca^{2+} inactivation of open Ca^{2+} channels. *Biophys. J.* 58:985–995.

Simon, S. M., and R. Llinás. 1985. Compartmentalization of the submembrane Ca^{2+} activity during Ca^{2+} influx and its significance in transmitter release. *Biophys. J.* 48:485–498.

Smith, G. D. 1985. Numerical Solution of Partial Differential Equations: Finite Difference Methods. Oxford Applied Mathematics and Computing Science Series, 3rd edition. Clarendon Press, Oxford.

Stern, M. D. 1992. Buffering of Ca^{2+} in the vicinity of a channel pore. *Cell Calcium.* 13:183–192.

Tse, A., F. W. Tse, and B. Hille. 1994. Calcium homeostasis in identified pituitary gonadotrophs. *J. Physiol. (Lond.).* 477:511–525.

Tsien, R. Y. 1980. New Ca^{2+} indicators and buffers with high selectivity against magnesium and protons: design, synthesis, and properties of prototype structures. *Biochemistry.* 19:2396–2404.

Tsien, R. Y. 1989. Intracellular measurements of ion activities. *Annu. Rev. Biophys. Bioeng.* 12:227–253.

Tsugorka, A., E. Ríos, and L. A. Blatter. 1995. Imaging elementary events of Ca^{2+} release in skeletal muscle cells. *Science.* 269:1723–1726.

Wagner, J., and J. Keizer. 1994. Effects of rapid buffers on Ca^{2+} diffusion and Ca^{2+} oscillations. *Biophys. J.* 67:447–456.

Yao, Y., J. Choi, and I. Parker. 1995. Quantal puffs of intracellular Ca^{2+} evoked by IP_3 in *Xenopus* oocytes. *J. Physiol. (Lond.).* 482:533–553.

Zhou, Z. A., and E. Neher. 1993. Mobile and immobile Ca^{2+} buffers in bovine adrenal chromaffin cells. *J. Physiol. (Lond.).* 469:245–273.

Zweifach, A. Z., and R. S. Lewis. 1995. Rapid inactivation of depletion-activated Ca^{2+} current (I_{CRAC}) due to local Ca^{2+} feedback. *J. Gen. Physiol.* 105:209–206.